INTERNATIONAL JOURNAL FOR NUMERICAL METHODS IN ENGINEERING

Int. J. Numer. Meth. Engng 2010; **00**:1–29 *Prepared using* nmeauth.cls *[Version: 2000/01/19 v2.0]*

Higher-order extended finite elements with harmonic enrichment functions for complex crack problems

S. E. Mousavi[1] and E. Grinspun[2] and N. Sukumar[1,*]

[1] *Department of Civil and Environmental Engineering, University of California, Davis, CA 95616, USA*

[2] *Department of Computer Science, Columbia University, New York, NY 10027, USA*

SUMMARY

In this paper, we analyze complex crack problems in elastic media using harmonic enrichment functions in a higher-order extended finite element implementation. The numerically computed enrichment function of a crack is the solution of the Laplace equation with discontinuous Dirichlet boundary condition along the crack, and its interaction with branches or other cracks is realized by imposing vanishing Neumann boundary conditions along those cracks. The classical finite element displacement approximation is enriched by adding the enrichment function of a crack through the framework of partition of unity. A nested subgrid mesh is used in the Laplace solve with a rasterized approximation of a crack, which simplifies the numerical integration—no partitioning of finite elements is required. Harmonic enrichment functions readily permit the extension to handle multiple interacting and branched cracks without any special treatment around the junction points. Several numerical examples are presented that affirm the accuracy and effectiveness of the method when applied to complex crack configurations under mixed-mode loading conditions.

*Correspondence to: N. Sukumar, Department of Civil and Environmental Engineering, University of California, One Shields Avenue, Davis, CA 95616. E-mail: nsukumar@ucdavis.edu

KEY WORDS: harmonic enrichment, intersecting cracks, branched crack, closely interacting cracks, partition of unity method, extended finite element method, stress intensity factors

1. INTRODUCTION

In the finite element method (FEM), conforming elements are used to model discontinuities in the displacement field for fracture analyses. The elements in the vicinity of the crack-tip must be refined to capture the singular stress field and as the crack grows, remeshing is required to model the advance of the crack front. The extended finite element method (X-FEM) [1, 2] takes advantage of a priori knowledge about the asymptotic solution for crack problems by locally adding discontinuous and/or crack-tip asymptotic functions to the approximation through the framework of partition of unity. This enables the modeling of cracks without the need for remeshing, and optimal convergence rates are realized [3, 4]. Modeling branched and intersecting cracks is also possible using the X-FEM by introducing the junction enrichment function, which must be added to the solution space to represent the displacement field around the junction point [5–8]. Introduction of the junction function is problem-dependent and requires additional checks in the implementation when cracks branch or coalesce. In the X-FEM, stiffness matrix calculation over enriched elements involves numerical integration of discontinuous and/or singular functions. Integration of discontinuous functions is handled in one of several ways: integration over partitions [2], integration of equivalent polynomials [9], quadratures with variable weights [10], conformal mapping [11], or generalized Gaussian quadrature for discontinuous functions [12, 13]. For singular crack-tip functions, higher-order quadratures [2] or singular mapping over the partitions [3, 4, 13–15]

is used. Numerical integration can be particularly cumbersome when dealing with multiple intersecting or branched cracks. Using harmonic enrichment functions simplifies the numerical integration and a single approach emanates for accurate integration over the enriched elements, regardless of the cracks configuration or crack-element interaction.

Kaufmann et al. [16] proposed a new enrichment scheme in which the numerical enrichment function of a crack is obtained through the solution of the Laplace equation with suitable boundary conditions. The resulting (harmonic) enrichment function naturally generalizes to the case of branched and intersecting cracks without any special considerations about the junction point. Mousavi et al. [17] used the harmonic enrichment function to model cracks in an extended finite element setting. Herein, we refer to this implementation as harmonic X-FEM or HX-FEM. In this paper, we apply the higher-order HX-FEM (see References [4, 8, 18, 19] for previous studies on higher-order X-FEM) to complex crack geometries and show that harmonic enrichment functions provide a unifying procedure for modeling cracks with notable simplifications in the implementation.

A brief description of the extended finite element method is given in Section 2. The algorithm for constructing the harmonic enrichment functions is described with an illustrative example in Section 3. Accurate numerical integration and quadrature requirements in the HX-FEM are addressed in Section 4.1, and in Section 4.2, the rate of convergence of HX-FEM with higher-order elements is studied. Several numerical examples, including cracks with complex geometries, multiple closely interacting cracks and an array of branched cracks are solved and the stress intensity factors (SIFs) are presented in Section 5. We close with our main findings and a few final remarks in Section 6.

2. EXTENDED FINITE ELEMENT METHOD

Consider the domain Ω with boundary $\Gamma = \Gamma_u \cup \Gamma_t \cup \Gamma_c$. The displacement boundary condition is prescribed over Γ_u and the traction is prescribed over Γ_t. The boundary Γ_c is composed of all crack faces that are assumed to be traction-free. The strong form for elastostatics is:

$$\begin{aligned} \boldsymbol{\nabla} \cdot \boldsymbol{\sigma} &= \mathbf{0} \text{ in } \Omega \\ \mathbf{u} &= \bar{\mathbf{u}} \text{ on } \Gamma_u \\ \boldsymbol{\sigma} \cdot \mathbf{n} &= \bar{\mathbf{t}} \text{ on } \Gamma_t \\ \boldsymbol{\sigma} \cdot \mathbf{n} &= \mathbf{0} \text{ on } \Gamma_c, \end{aligned} \tag{1}$$

where $\boldsymbol{\sigma}$ is the Cauchy stress tensor, $\mathbf{u}$ is the displacement, $\mathbf{n}$ is the unit outward normal and $\bar{\mathbf{u}}$ and $\bar{\mathbf{t}}$ are the prescribed displacements and tractions on Γ_u and Γ_t, respectively. On using the linear elastic constitutive law $\boldsymbol{\sigma} = \mathbf{C} : \boldsymbol{\varepsilon}$, the weak form of the boundary-value problem in (1) is: find $\mathbf{u} \in \mathcal{U}$ such that

$$\int_\Omega \boldsymbol{\varepsilon}(\mathbf{u}) : \mathbf{C} : \boldsymbol{\varepsilon}(\mathbf{v}) d\Omega = \int_{\Gamma_t} \bar{\mathbf{t}} \cdot \mathbf{v} d\Gamma \ \forall \mathbf{v} \in \mathcal{U}_0, \tag{2}$$

where $\mathcal{U}$ and $\mathcal{U}_0$ are the trial and test spaces, which include functions that are discontinuous across Γ_c, $\boldsymbol{\varepsilon}$ is the small-strain tensor, and $\mathbf{C}$ is the material moduli tensor. After discretizing the domain, the trial function in the extended finite element method takes the following general form [5]:

$$\begin{aligned} \mathbf{u}^h(\mathbf{x}) = &\sum_{I \in \mathcal{N}} N_I(\mathbf{x}) \mathbf{u}_I + \sum_{c=1}^{n_c} \sum_{I \in \mathcal{N}_c} N_I(\mathbf{x}) H_c(\mathbf{x}) \mathbf{a}_{Ic} \\ &+ \sum_{t=1}^{n_t} \sum_{I \in \mathcal{N}_t} \sum_{\alpha=1}^{4} N_I(\mathbf{x}) \Phi_{\alpha t}(\mathbf{x}) \mathbf{b}_{I\alpha t} + \sum_{j=1}^{n_j} \sum_{I \in \mathcal{N}_j} N_I(\mathbf{x}) J_j(\mathbf{x}) \mathbf{c}_{Ij}, \end{aligned} \tag{3a}$$

with

$$\{\mathbf{\Phi}_{\alpha t}(\mathbf{x})\}_{\alpha=1}^{4} = \left\{\sqrt{r}\sin\frac{\theta}{2}, \sqrt{r}\cos\frac{\theta}{2}, \sqrt{r}\sin\theta\sin\frac{\theta}{2}, \sqrt{r}\sin\theta\cos\frac{\theta}{2}\right\}, \tag{3b}$$

where $\mathcal{N}$ is the set of all nodes in the mesh, $\mathcal{N}_c$ is the set of nodes whose shape function support is cut by the interior of the crack c, $\mathcal{N}_t$ is the set of nodes whose shape function support contains the crack-tip t and $\mathcal{N}_j$ is the set of nodes that are enriched for the junction j. In addition, $N_I(\mathbf{x})$ are the finite element shape functions, $H_c(\mathbf{x})$ is the generalized Heaviside function defined with respect to crack c, $\Phi_{\alpha t}(\mathbf{x})$ in (3b) are the crack-tip asymptotic functions defined with respect to crack-tip t (r and θ are the polar coordinates of a point in the coordinate system attached to the crack-tip), $J_j(\mathbf{x})$ is the junction function corresponding to the jth junction. The unknown coefficients of node I corresponding to the classical, Heaviside, near-tip and junction shape functions are $\mathbf{u}_I$, $\mathbf{a}_{Ic}$, $\mathbf{b}_{I\alpha t}$ and $\mathbf{c}_{Ij}$, respectively. The number of cracks, crack-tips and junctions present in the domain are indicated by n_c, n_t and n_j, respectively.

In (3), multiple near-tip and junction enrichment functions are required in addition to the generalized Heaviside function to realize the correct displacement field in the presence of a crack and its interactions with other existing cracks in the domain. On the other hand, the harmonic enrichment function for a given crack is computed by considering its interactions with its branches and all other intersecting cracks. Thus, flexibility accrues and the complexity of the implementation is also reduced. The extended finite element approximation for crack modeling with harmonic enrichment functions is [17]:

$$\mathbf{u}^h(\mathbf{x}) = \sum_{I\in\mathcal{N}} N_I(\mathbf{x})\mathbf{u}_I + \sum_{c=1}^{n_c}\sum_{I\in\mathcal{N}_c} N_I(\mathbf{x})\psi_c(\mathbf{x})\mathbf{a}_{Ic}, \tag{4}$$

where $\psi_c(\mathbf{x})$ is the harmonic enrichment function of crack c. On substituting the trial and test approximations of the form (4) into (2), and using the arbitrariness of nodal variations, the

discrete system of equations are obtained.

3. HARMONIC ENRICHMENT FUNCTIONS

We construct the harmonic enrichment function of a crack via the solution of the Laplace equation [16]:

$$\Delta\psi_c(\mathbf{x}) = 0 \ \text{ in } \Omega_c^\ell, \tag{5}$$

with appropriate boundary conditions. In (5), ψ_c is the enrichment function of crack c, Δ is the Laplacian operator and Ω_c^ℓ contains all the elements that are enriched for crack c and is called the Laplace domain of crack c. Solving the Laplace equation is a separate problem that is done over a different discretization ($\mathcal{D}_c^\ell$) and is independent of the discretization used for the elasticity problem ($\mathcal{D}$). One can solve the Laplace equation and obtain the numerical enrichment function by either finite differences as in Reference [16] or via finite elements as adopted in Reference [17] and herein. We illustrate the construction of the harmonic enrichment function through a sample problem with multiple cracks.

Consider the domain shown in Figure 1a with two cracks, one of which has a branch. The branched crack is modeled as a main crack, MON, and a branch OP. A sample discretization of the domain with linear quadrilateral elements is shown in Figure 1b. All the nodes whose basis function supports are cut by a crack, are enriched for the crack. In Figure 1b, the nodes that are enriched for cracks AB, MON and OP are marked with filled circles, empty squares and asterisks, respectively.

First, we construct the enrichment function for the crack AB, namely ψ_{AB}. The domain over which ψ_{AB} is evaluated during the element stiffness matrix calculations, is limited to the union of the elements that are enriched for this crack; hence, the Laplace domain for crack AB, Ω_{AB}^ℓ,

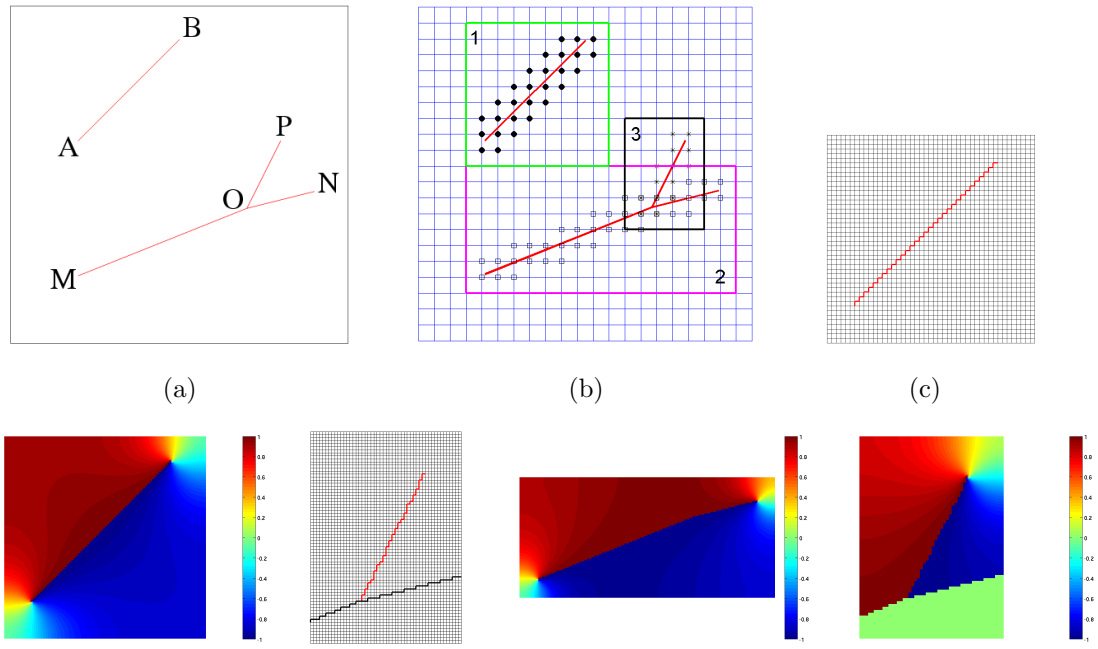

Figure 1. Algorithm for construction of harmonic enrichment functions. (a) geometry of the domain and crack configuration; (b) enriched nodes and Laplace domains; (c) subgrid mesh and *rasterized* approximation of the crack AB (Manhattan path); (d) enrichment function of crack AB; (e) subgrid mesh and rasterized approximation of the crack OP; (f) enrichment function of crack MON; and (g) enrichment function of crack OP.

must be selected so that it covers all of the elements that are enriched for the crack AB. For simplicity, we choose the Laplace domain of a crack, as the smallest box that contains all the elements that are enriched for the corresponding crack (box 1 in Figure 1b). Note that there is a minor difference between the way we pick Ω^{ℓ}_{AB} and the way it was decided in Reference [17]: we choose a more compact domain for the Laplace equation, resulting in a faster solution without loss of accuracy. The Laplace domain is discretized with $m \times m$ subelements over each enriched element (nested discretization). We refer to the the discretization for crack AB as $\mathcal{D}^{\ell}_{\mathcal{AB}}$. The crack-path Γ_{AB} is approximated with a zigzag line (called rasterized approximation or Γ^{r}_{AB}) that passes through the subelements of $\mathcal{D}^{\ell}_{\mathcal{AB}}$ but does not cut them (see Figure 1c). In order to model the discontinuity along the crack segments, the harmonic enrichment function must be discontinuous along Γ^{r}_{AB}. To realize the discontinuity, the nodes of the Laplace mesh that coincide with Γ^{r}_{AB} are duplicated and the connectivity of the subelements is modified so that the ones above and below the crack are connected to distinct copies of a node with the same coordinates. Dirichlet boundary conditions are imposed over the duplicated nodes: $\psi_{AB} = +1$ and $\psi_{AB} = -1$ are assigned to the duplicated nodes above and below the crack, respectively, and $\psi_{AB} = 0$ is assigned to the crack-tip node(s). At this point, if Ω^{ℓ}_{AB} contains any other crack, for example, in the case of intersecting, closely interacting, or branched cracks, a vanishing Neumann boundary condition must also be imposed along those cracks. To realize this condition, the rasterized path of the interacting cracks are also extracted and the nodes of the domain that coincide with the zigzag crack-path are duplicated. The subelements of $\mathcal{D}^{\ell}_{\mathcal{AB}}$ are all alike which makes it possible to calculate the element stiffness matrix for one and insert it into the appropriate rows and columns of the Laplace stiffness matrix. After setting up the Laplace mesh and boundary conditions, a linear solver is used to obtain the

numerical enrichment function. Since the domain of the Laplace equation is restricted to the crack size, the calculation of the harmonic enrichment function only entails a fraction of the total computational cost for the problem. The enrichment function of crack AB is depicted in Figure 1d.

The Laplace domain for the crack OP, i.e., Ω^{ℓ}_{OP}, is box 3 in Figure 1b and its discretization, $\mathcal{D}^{\ell}_{\mathcal{OP}}$, is shown in Figure 1e. After setting the Dirichlet boundary conditions for Γ^{r}_{OP}, it is observed that Ω^{ℓ}_{OP} contains the crack MON, in addition to the branch OP. Therefore, Γ^{r}_{MON} is found and the nodes of $\mathcal{D}^{\ell}_{\mathcal{OP}}$ that coincide with Γ^{r}_{MON} are duplicated to realize a zero Neumann boundary condition along the crack MON. Γ^{r}_{OP} and Γ^{r}_{MON} are shown in Figure 1e with zigzag lines. The enrichment function of cracks MON and OP are shown in Figures 1f and 1g, respectively. Note that in Figure 1g the enrichment function of the branch automatically takes on the form of the junction function of Daux et al. [5] in the region close to the branching point; whereas far from it, the generalized Heaviside function is reproduced. Consequently, a unified procedure emerges to construct the enrichment function for all the cracks with no special considerations for the branched crack or the near-tip region.

The algorithm that follows summarizes the construction of the harmonic enrichment function.

Algorithm: Construction of the harmonic enrichment function

Input: domain of the problem Ω with the discretization $\mathcal{D}$ using quadrilateral finite elements; *numc* cracks $\{\Gamma_i\}_{i=1}^{numc}$; number of divisions over each enriched element $m \times m$

Output: harmonic enrichment function of crack c, ψ_c, which is numerically computed over its corresponding discretization $\mathcal{D}^{\ell}_{c}$

1. Find Ω^{ℓ}_{c}: the smallest box containing all the elements enriched for crack c.

2. Discretize Ω_c^ℓ using $m \times m$ subelements over each enriched element and obtain $\mathcal{D}_c^\ell$.
3. Find Γ_c^r: the rasterized approximation of crack c over $\mathcal{D}_c^\ell$.
4. If Ω_c^ℓ contains any other crack, find their rasterized approximation as well: $\{\Gamma_i^r\}_{i\in I_c}$ with I_c being the set of cracks interacting with crack c.
5. Duplicate all nodes of $\mathcal{D}_c^\ell$ that are coincident with Γ_c^r and change the connectivity of the subelements of $\mathcal{D}_c^\ell$ so that the subelements above and below Γ_c^r are connected to distinct copies of the nodes.
6. For the nodes in Γ_c^r and their copies, assign the Dirichlet boundary condition: $\psi_c = +1$ for the nodes connected to the subelements above Γ_c^r and $\psi_c = -1$ for the ones below Γ_c^r. If crack c has a tip(s), assign $\psi_c = 0$ for the tip node(s).
7. Repeat step 5 for the cracks $\{\Gamma_i^r\}_{i\in I_c}$.
8. Solve the Laplace equation with the prescribed Dirichlet and Neumann boundary conditions and get ψ_c.

We described the algorithm for constructing harmonic enrichment functions for quadrilateral elements and subelements used for discretizing Ω and Ω_c^ℓ. The reader can readily infer that generalizing the algorithm to other types of elements, such as triangular or polygonal elements, is straightforward and needs minor changes to the above algorithm.

4. NUMERICAL INTEGRATION AND CONVERGENCE STUDY

4.1. Numerical integration

A well-known issue in partition of unity methods with non-polynomial enriched basis functions is the numerical integration of the basis function derivatives. In the X-FEM, the gradient of

the enrichment functions has discontinuities and/or singularities; therefore, the computation of stiffness matrix entries in enriched elements requires additional care. Some of the methods for the integration of discontinuous functions include integration by dividing the elements into conforming partitions [2], integrating equivalent continuous polynomials [9], integration using quadratures with variable weights [10], conformal mapping over the cut elements [11], and generalized Gaussian quadratures for discontinuities [12, 13]. Similarly, the integration of the singular functions over the crack-tip elements can be done using higher-order standard Gaussian quadratures [2]. However, more efficient and accurate results can be obtained by using transformations that resolve the singularity [3, 4, 13–15]. By contrast, the harmonic enrichment function is the finite element solution of the Laplace equation: it is a piecewise bilinear function within the subgrid elements, and hence integration of the weak form in the HX-FEM can be done *exactly* using standard Gauss quadratures over the subgrid and there is no need to introduce special quadrature rules over the enriched elements.

In general, an entry of the stiffness matrix of an element corresponding to the degrees of freedom i and j can be written as:

$$k_{ij} = \int_{\Omega_e} \mathbf{B}_i^T \mathbf{C} \mathbf{B}_j dV, \tag{6}$$

where $\mathbf{C}$ is the material constitutive matrix, and $\mathbf{B}_i$ and $\mathbf{B}_j$ are the derivatives of the shape functions corresponding to the extended degrees of freedom i and j. The material matrix is a constant matrix for linear elastic fracture mechanics and for simplicity we replace it with the identity matrix. On assuming i and j to be enriched degrees of freedom, (6) can be written as:

$$k_{ij} = \int_{\Omega_e} \nabla(N_i \psi) \cdot \nabla(N_j \psi) dV, \tag{7}$$

where ψ is the harmonic enrichment function, which is bilinear with respect to x and y, and N_i and N_j are the classical finite element shape functions. In this study, we adopt bilinear

quadrilateral ($Q4$), biquadratic (serendipity) quadrilateral ($Q8$), and bicubic (serendipity) quadrilateral ($Q12$) elements. The integrand of (7) has maximum orders (in each coordinate direction) of 4, 6 and 8 for $Q4$, $Q8$ and $Q12$ finite elements, respectively. As a result, 3×3, 4×4 and 5×5 tensor-product rules over the subgrid are needed for exact integration over bilinear, biquadratic, and bicubic elements, respectively. When i and/or j are classical degrees of freedom, the term ψ is not present in (7), and a lower order quadrature suffices. Although this is the requirement for exact numerical integration of the weak form, the error of the numerical integration scheme is only required to be lower than the approximation error of the method—a less-accurate quadrature may be adequate. To clarify this issue, we perform a systematic study to determine the minimal quadrature in the HX-FEM.

Consider the well-known problem of an oblique center-crack in an infinite plate under biaxial loading. The crack has unit length and is inclined at an angle of 45°. This problem has an analytical solution [20] and has been solved using X-FEM [13, 21] and HX-FEM [17]. The goal here is to find the minimum quadrature requirement for different subgrid refinements and element types so that the accuracy of SIF calculations is not compromised. The stress intensity factors are calculated and presented in Figure 2 for bilinear, biquadratic and bicubic elements and different levels of subgrid refinement. It is observed that a 2×2 tensor-product quadrature rule over the subgrid is sufficient to obtain accurate SIFs. In the convergence study of Section 4.2 and in the numerical examples in Section 5, a 2×2 Gauss quadrature rule is used over each subelement of the subgrid mesh.

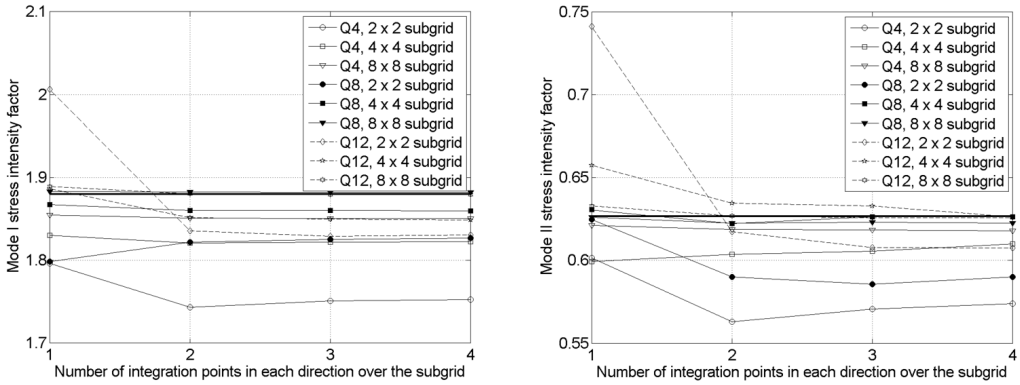

(a) (b)

Figure 2. Inclined center-crack in an infinite plate: convergence of stress intensity factors with number of integration points in each direction over the subgrid. A 40×40 mesh with bilinear, biquadratic and bicubic elements is used. (a) Mode I stress intensity factor; and (b) Mode II stress intensity factor. The thick solid lines represent the exact solutions.

4.2. Convergence study

Convergence of the HX-FEM for bilinear elements was studied in Reference [17], and a rate of convergence of one-half in the energy norm was realized for fracture problems. The sub-optimal rate of convergence is attributed to the fact that the harmonic enrichment function does not reproduce all the terms that are present in the displacement field around the crack-tip, whereas in the X-FEM with topological enrichment [3, 4], the analytic near-tip functions are added to the solution space in a fixed area around the crack-tip, and as a result, the optimal rate of convergence is recovered. Here, we study the convergence of HX-FEM for $Q8$ and $Q12$ elements, using the same problem that was considered in Reference [17].

Consider the rectangular plate covering the region $(-1, 1) \times (-1, 1)$ with a crack defined as the line segment $(-1, 0) - (0, 0)$. Young's modulus $E = 1$ and the Poisson ratio $\nu = 0$

are assumed for the material of the plate. Dirichlet boundary condition is assumed over the four edges of the plate: mode I displacement field, corresponding to $K_I = 1$ and $K_{II} = 0$ (discontinuous along the crack) is imposed over the edges of the plate. The relative energy norm of the error is evaluated as:

$$E_{rel} = \frac{||\mathbf{u} - \mathbf{u}^h||_{E(\Omega)}}{||\mathbf{u}||_{E(\Omega)}} = \frac{\left(\int_\Omega (\boldsymbol{\varepsilon} - \boldsymbol{\varepsilon}^h)^T \, \mathbf{C} \, (\boldsymbol{\varepsilon} - \boldsymbol{\varepsilon}^h) d\Omega\right)^{1/2}}{\left(\int_\Omega \boldsymbol{\varepsilon}^T \, \mathbf{C} \, \boldsymbol{\varepsilon} d\Omega\right)^{1/2}}, \tag{8}$$

where $\mathbf{u}$ and $\mathbf{u}^h$ are the exact and extended finite element solutions for the displacement field, $\boldsymbol{\varepsilon}$ and $\boldsymbol{\varepsilon}^h$ are the exact and extended finite element solutions for the strain tensor, and $\mathbf{C}$ is the constitutive matrix. A sequence of meshes is considered: 10×10, 20×20, 40×40, 80×80 and 160×160, with a 6×6 subgrid over the enriched elements, to calculate the harmonic enrichment function. See Figure 3a for a sample mesh and the corresponding enriched nodes. The relative error in the energy norm is depicted in Figure 3b for linear, quadratic and cubic elements, and rates of convergence of 0.499, 0.502 and 0.502, respectively, are realized. The rates of convergence agree with finite element theory for the solution of $\sqrt{r}$-singular problems. The absolute error is reduced when higher-order elements are used, but the rate of convergence is not improved. Similar rates of convergence are obtained when a 3×3 subgrid is used for the enrichment function computations; however, the absolute error in the energy norm is greater in this case.

5. NUMERICAL RESULTS

In this section, we present several numerical examples to show the capabilities of adopting harmonic enrichment functions in the X-FEM. Our examples include multiple collinear cracks, large zigzag cracks, array of branched cracks and finally multiple closely interacting cracks. In

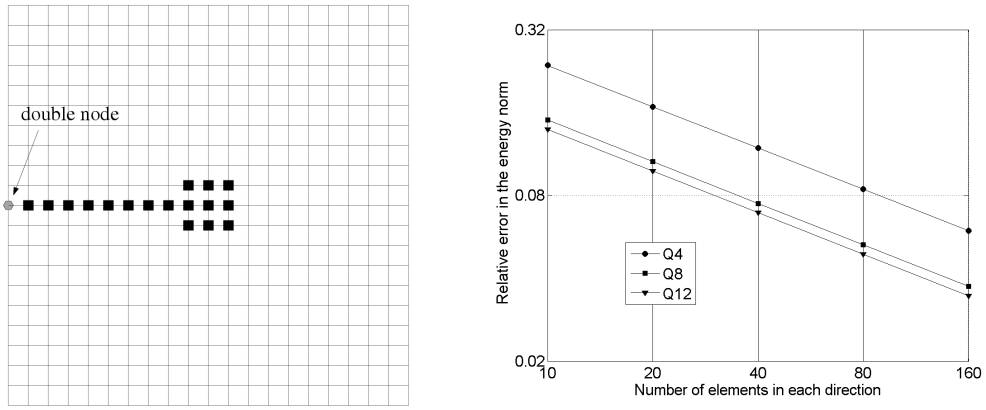

(a) (b)

Figure 3. Convergence of the HX-FEM with linear, quadratic and cubic elements. (a) enriched nodes; and (b) relative energy norm of the error for $Q4$, $Q8$ and $Q12$ elements.

order to discretize the domain, we use bilinear and biquadratic finite elements. In the following subsections, whenever the so-called standard version of the X-FEM with the generalized Heaviside function and near-tip asymptotic functions is used, it is labeled as X-FEM; and whenever the harmonic enrichment function is used, it is called HX-FEM. In all the examples, the material is assumed to be homogeneous and isotropic with Young's modulus $E = 10^5$ and Poisson's ratio $\nu = 0.3$. Plane strain condition is used for the examples in Sections 5.1 to 5.4 and plane stress condition is assumed for the example in Section 5.5.

5.1. Three collinear cracks in a large finite plate

First, we solve the problem of three collinear cracks at the middle of a plate and two ligaments between the interior crack tips. The plate is under uniaxial loading perpendicular to the crack direction as shown in Figure 4a. In an infinite plate, this problem admits an exact solution [22]. We consider a large finite plate with dimensions 400×400 and crack half-length of $a = 1$ with

Table I. Normalized mode I stress intensity factor for three collinear cracks in a large finite plate.[a]

SIFs	X-FEM		HX-FEM[b]	
	Q4	Q8	Q4	Q8
K_I^A/K_I^{A*}	0.975	0.989	0.971	0.985
K_I^B/K_I^{B*}	0.988	0.991	0.970	0.982
K_I^C/K_I^{C*}	0.990	0.991	0.965	0.991

[a] Reference solution: $K_I^{A*} = 1.9679$, $K_I^{B*} = 2.2749$ and $K_I^{C*} = 2.3421$ [23].

[b] Each enriched finite element is divided into 3×3 subgrid elements.

ligament length $k = 1/2$, similar to the one solved by Yavuz et al. [23]. Since the domain is very large with respect to the crack dimensions, we use a Cartesian refinement of the mesh: larger element size is used in the region far from the cracks, and in the vicinity of the cracks smaller elements are employed so that a compromise between accuracy and efficiency is attained. A sample of the discretization of the domain is illustrated in Figures 4b and 4c. The harmonic enrichment function is shown in Figure 4d. The numerical results for the SIFs are given in Table I which show good agreement with the ones obtained by Yavuz et al. [23].

5.2. Zigzag edge-crack in a semi-infinite plate

Consider a zigzag edge-crack in a semi-infinite plate under uniaxial loading as shown in Figure 5a. The crack has N segments, each of which has a length of a and makes an angle of 45° with the horizontal. A uniform mesh with 400 linear elements in each direction is used over the entire domain and the domain size is increased until the results converge to the ones from the semi-infinite domain. We solve the case of $N = 6$ segments and a domain size of 160×160 is taken for a crack-segment length of $a = 1$ to adequately represent a semi-infinite domain.

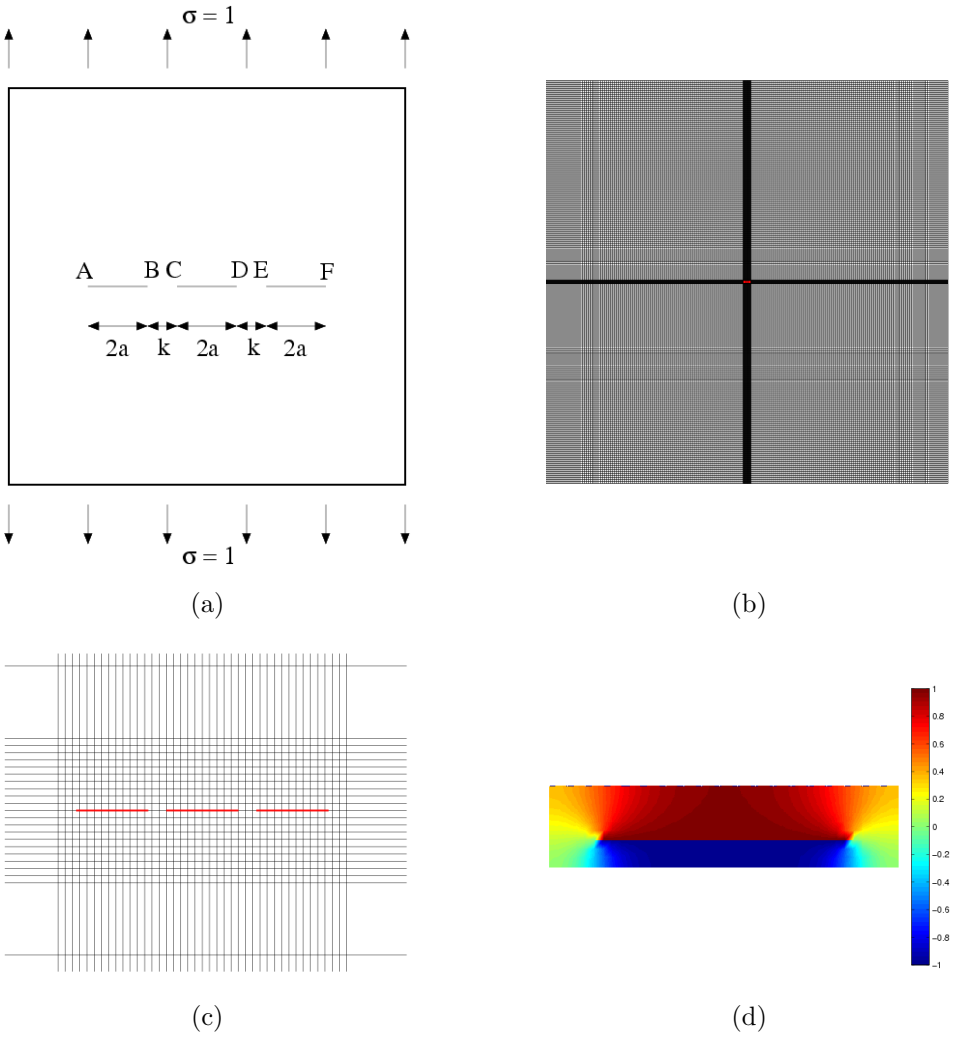

Figure 4. Three collinear cracks in a large finite plate. (a) geometry; (b) sample mesh; (c) Cartesian refinement near the cracks; and (d) typical harmonic enrichment function.

The harmonic enrichment function is depicted in Figure 5b with a 3×3 refinement over each enriched element to obtain the mesh for the Laplace solve. This problem has been considered by Brandinelli and Ballarini [24] using the singular integral method with/without a three-segment approximation to the crack-path instead of considering the whole crack geometry. We

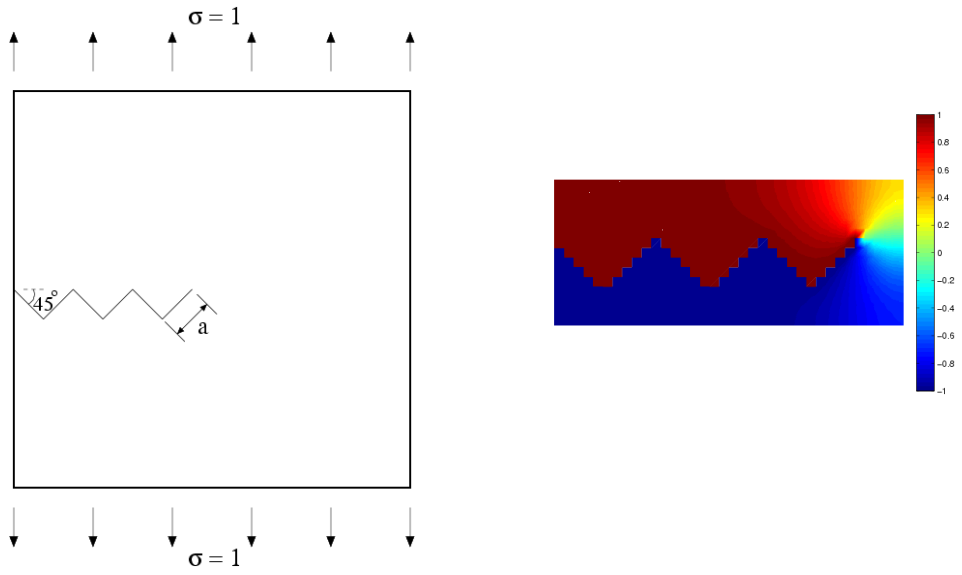

(a) (b)

Figure 5. Zigzag edge-crack in a semi-infinite plate. (a) geometry; and (b) harmonic enrichment function.

Table II. Normalized stress intensity factors for a zigzag edge-crack in a semi-infinite plate.[a]

SIFs	X-FEM	HX-FEM		
		subgrid 3×3	subgrid 6×6	subgrid 10×10
K_I/K_I^*	1.018	0.990	0.995	0.997
K_{II}/K_{II}^*	0.994	0.968	0.979	0.985

[a] Reference solution: $K_I^* = 3.069$ and $K_{II}^* = 1.510$ [25].

compare our results in Table II with those from Reference [25].

5.3. Large zigzag crack in an infinite plate

To further explore the capability of the harmonic enrichment function to resolve the displacement field around a crack with a complicated geometry, we analyze an infinite plate with a large zigzag crack with many segments under uniaxial loading perpendicular to the crack direction (see Figure 6a for the geometry of the problem and loading). The straight part of the crack has a length $2a$ and the first inclined segment has a length a. All other segments have a length of $2a$ and the inclined segments make an angle of 45° with the horizontal. Englund [26] applied the singular integral method to solve this problem with N corners when $N = 10$ and $N = 100$. To represent the infinite domain, we set the plate size to 200×200 for $N = 10$ and 1600×1600 for $N = 100$ and discretize the domain with linear elements that are finer around the zigzag crack and larger far from it. For the case $N = 10$, we choose the element size $h_e = 4$ far from the cracks and $h_e = 0.25$ in the vicinity of the cracks. For the larger crack with $N = 100$ corners, $h_e = 8$ and $h_e = 0.25$ are used.

The calculated SIFs for the right crack-tip are given in Table III for a subgrid of 3×3 over each enriched element, and are found to be in excellent agreement with the results of Englund [26]. We also present the SIFs for more refined elements in Table III for the case $N = 10$. It is observed that our results approach those of the reference solution. The enrichment function for $N = 10$ is shown in Figure 6b.

5.4. Multiple closely interacting cracks in a finite plate

In this example we apply the HX-FEM to analyze a finite plate with multiple closely interacting cracks with kinks and branches, which is considered in Reference [23]. A schematic description of the geometry of the problem is given in Figure 7a. The coordinates of the points A to J

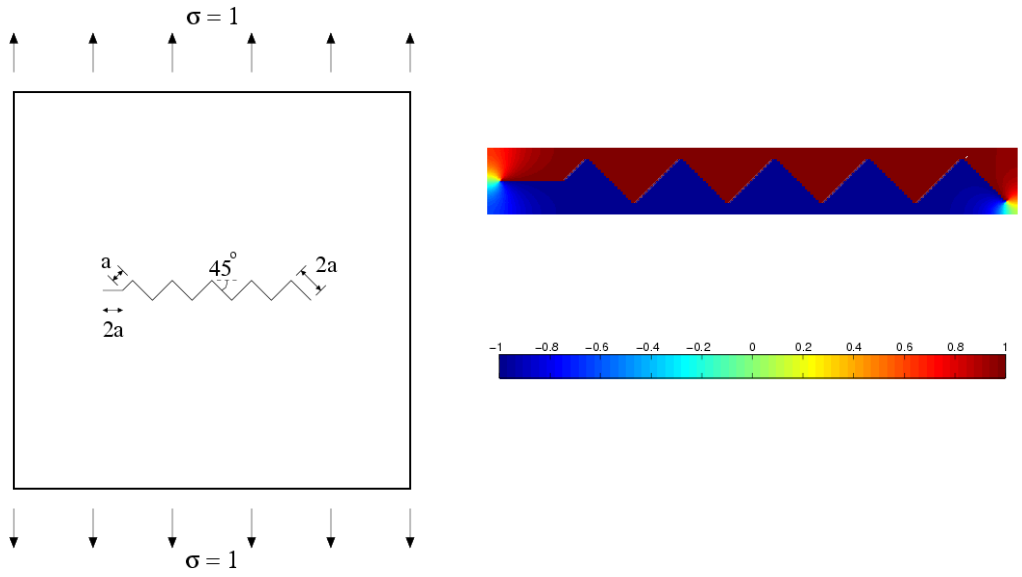

(a) (b)

Figure 6. Large zigzag crack in an infinite plate. (a) geometry: plate size is $L \times L$; and (b) harmonic enrichment function for $N = 10$.

Table III. Normalized stress intensity factors for the large zigzag crack in an infinite plate.[a]

Problem	Mesh	SIFs	X-FEM	HX-FEM
$N = 10$, $L = 200$	$h_e = [4, 0.25]$	K_I/K_I^*	1.005	0.990
	$numel = 140 \times 80$	K_{II}/K_{II}^*	1.018	0.984
	$h_e = [2, 0.125]$	K_I/K_I^*	0.998	0.997
	$numel = 250 \times 130$	K_{II}/K_{II}^*	1.011	0.997
$N = 100$, $L = 1600$	$h_e = [8, 0.25]$	K_I/K_I^*	1.004	0.996
	$numel = 820 \times 262$	K_{II}/K_{II}^*	1.018	0.992

[a] Reference solution: $K_I^* = 3.323$ and $K_{II}^* = -2.213$ for $N = 10$ and $K_I^* = 11.279$ and $K_{II}^* = -5.338$ for $N = 100$ [26].

and A' to J' that define the cracks are listed in Table IV. The plate is under mixed-mode biaxial tension and shear loadings. We solve the problem for two different plate sizes: 20×20 and 40×40; and discretize it using bilinear and biquadratic elements. Since the cracks are concentrated in the center of the plate, we use a Cartesian refinement around the cracks with an element size $h_e = 0.02$, and use $h_e = 0.52$ elsewhere. For a sample discretization of the domain see Figure 7b. In Figure 7c, the enriched nodes are marked with open squares and asterisks for the main cracks and branches, respectively. We use two subgrid refinements: each enriched element is subdivided into 3×3 and 6×6 subelements to obtain the Laplace discretization. Note that to calculate the enrichment function of each of the cracks, the union of the elements that are enriched only for that crack is considered. Hence, the size of the Laplace domain to calculate the enrichment function of each of the cracks is limited to the region around that crack, and essential boundary conditions are imposed along the rasterized approximation of the crack (see Figure 7d). If this region contains any other crack, e.g., in the case of branched, intersecting or very close cracks, as one would expect, the vanishing natural boundary conditions are also imposed along all other cracks that are present. This algorithm results in multiple patches that cover enriched elements corresponding to each of the cracks. See the enrichment function of the cracks JC and $J'C'$ in Figure 7d for the case where the Dirichlet boundary condition is imposed along the branch and zero natural boundary condition is imposed along the main crack—the resulting enrichment functions resemble the junction function around the branching point.

Compared to the X-FEM, in the HX-FEM there is no need to partition the elements for the numerical integration and Gauss quadrature is used inside each subgrid. Also, it is noteworthy that our algorithm for the construction of the harmonic functions can be readily applied to

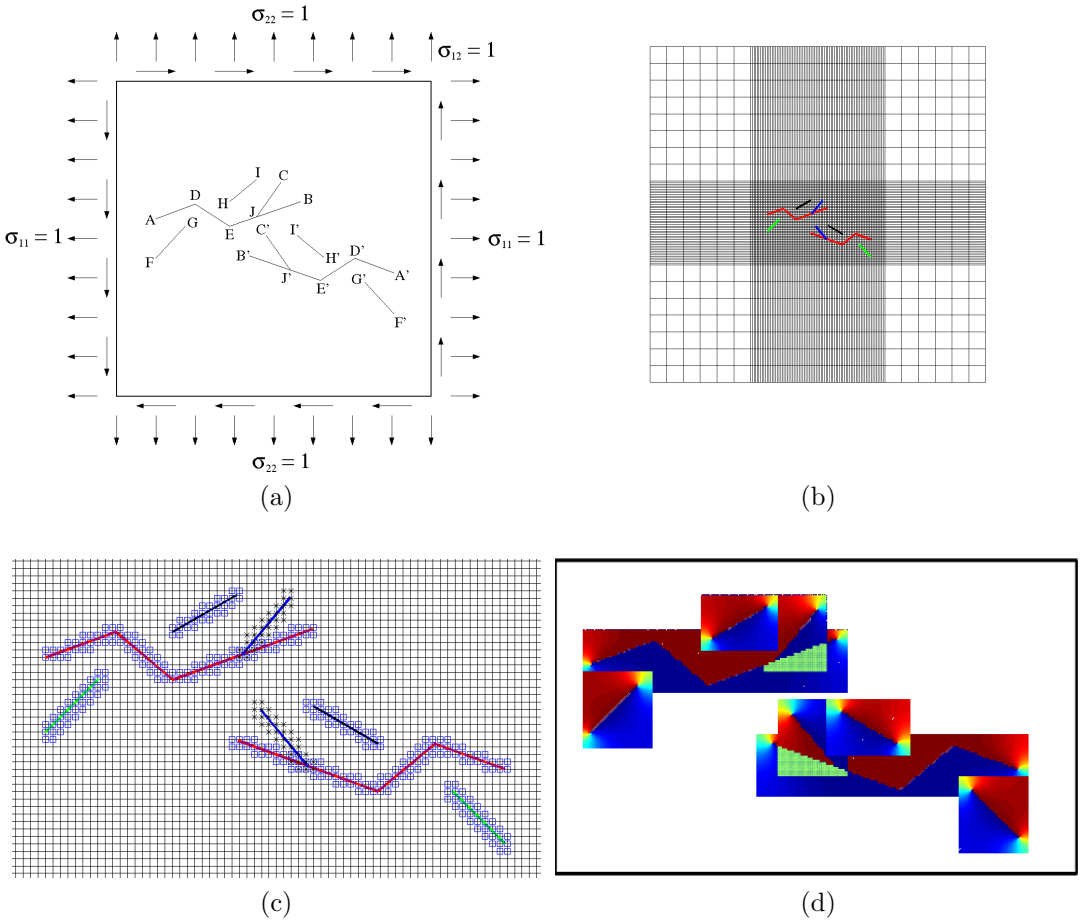

Figure 7. Multiple closely interacting cracks in a finite plate. (a) geometry; (b) a sample mesh with Cartesian refinement around the cracks; (c) enriched nodes; and (d) harmonic enrichment functions.

this problem without the need for any special treatment for multiple and/or branched cracks. We use $Q4$ and $Q8$ finite elements for the discretization of the domain. 3×3 and 6×6 subgrid elements are used over each enriched element to discretize the Laplace domain. The SIFs of crack-tips B, C, and G are calculated and normalized with respect to the reference solution of Yavuz et al. [23] (see Table V).

Table IV. Coordinates of the points that define the cracks in the interacting cracks problem.

Point	x	y	Point	x	y
A	0	0	A'	6.170245	-1.5
B	3.585122	0.383273	B'	2.585122	-1.116727
C	3.288217	0.807297	C'	2.882027	-0.692703
D	0.939693	0.342020	D'	5.230552	-1.157980
E	1.705737	-0.300767	E'	4.464508	-1.800767
F	0	-1	F'	6.170245	-2.5
G	0.707107	-0.292893	G'	5.463138	-1.792893
H	1.705737	0.342020	H'	4.464508	-1.157980
I	2.571762	0.842020	I'	3.598482	-0.657980
J	2.645430	0.041253	J'	3.524815	-1.458747

5.5. Array of branched cracks in a finite plate

The problem of multiple branched cracks in an infinite plate has been solved previously using the singular integral method [27] and the distributed dislocation approach [28], to name a few. Here, as the last example, we consider an array of branched cracks in a finite plate under uniaxial loading. Plane stress conditions are assumed, and the domain geometry and crack configuration is shown in Figure 8a. The cracks are considered as four main cracks, AOC, DPF, GQI and JRL and four branches OB, PE, QH and RK. Any other combination, for example, AO and BOC for the upper-left branched crack, could equivalently be used as demonstrated in Reference [17]. We discretize the domain with 301×301 uniform linear elements and use a 3×3 subgrid over each enriched element. The typical enrichment function

Table V. Normalized stress intensity factors for closely interacting cracks in a finite plate.[a]

			Crack-tip	B		C		G	
Plate size	Mesh	SIFs	Subgrid	Q4	Q8	Q4	Q8	Q4	Q8
20×20	$h_e = [0.52, 0.02]$	K_I/K_I^*	3×3	0.975	0.995	0.972	0.989	0.947	0.974
	$numel = 375 \times 225$		6×6	0.976	0.989	0.975	0.992	0.949	0.974
		K_{II}/K_{II}^*	3×3	0.961	0.958	1.002	0.979	1.008	0.981
			6×6	0.976	0.976	1.017	1.032	1.013	1.002
40×40	$h_e = [0.52, 0.02]$	K_I/K_I^*	3×3	0.977	0.997	0.977	0.990	0.955	0.975
	$numel = 400 \times 275$		6×6	0.978	0.990	0.980	0.993	0.959	0.977
		K_{II}/K_{II}^*	3×3	0.961	0.963	0.964	0.981	1.036	0.938
			6×6	0.975	0.976	0.981	1.009	1.036	0.992

[a] Reference solution for plate size 20×20: $K_I^{B*} = 1.9932$, $K_{II}^{B*} = 2.4042$, $K_I^{C*} = -1.6920$, $K_{II}^{C*} = -0.1337$, $K_I^{G*} = -0.5317$ and $K_{II}^{G*} = 0.1885$. Reference solution for plate size 40×40: $K_I^{B*} = 1.8181$, $K_{II}^{B*} = 2.2483$, $K_I^{C*} = -1.4996$, $K_{II}^{C*} = -0.1783$, $K_I^{G*} = -0.4943$ and $K_{II}^{G*} = 0.1119$. Reference solutions are from Yavuz et al. [23].

for a pair of cracks is shown in Figures 8b and 8c for a main crack and a branch, respectively. We compare our results with those obtained via the hypersingular formulation of the boundary element method (BEM) proposed by García et al. [29] where quadratic elements are used for each side of the external boundaries, discontinuous quadratic elements for the crack segments and quarter-point elements for the crack-tip elements (see Table VI). The calculated mode I and mode II SIFs of the crack-tips A to F are in good agreement with the reference solutions.

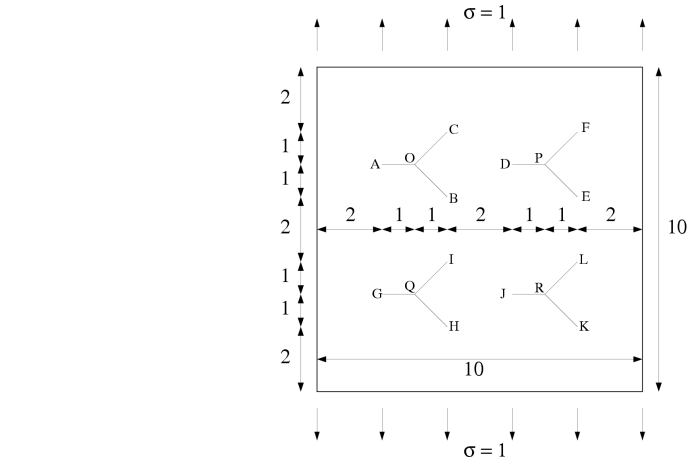

(a)

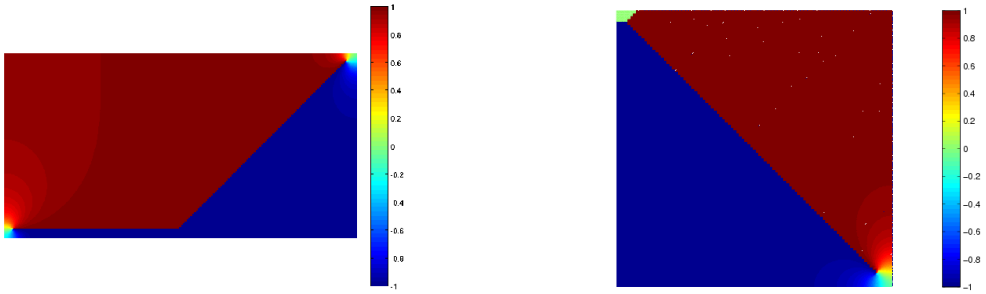

(b) (c)

Figure 8. An array of branched cracks in a finite plate. (a) geometry; and (b) and (c) typical harmonic enrichment functions of a main crack and a branch, respectively.

Table VI. Stress intensity factors for the array of branched cracks in a finite plate.

Crack-tip	A	B	C	D	E	F
$K_I^{*\,a}$	2.0925	1.0191	1.2117	2.2172	0.8176	1.1475
K_I/K_I^*	0.991	0.994	0.988	0.988	1.001	0.993
$K_{II}^{*\,a}$	0.08235	-0.9527	0.9989	-0.02288	-0.8929	1.0574
K_{II}/K_{II}^*	0.959	0.965	0.967	0.965	0.975	0.967

[a] Reference solution obtained via the boundary element method presented in Reference [29].

6. CONCLUDING REMARKS

In this paper, numerically constructed (harmonic) enrichment functions were used for crack modeling within the extended finite element method that automatically generalizes to the case of branched, intersecting and closely interacting cracks. Coding the harmonic X-FEM (HX-FEM) is straightforward and does not involve accounting for specific scenarios that arise as cracks branch or coalesce. We construct the enrichment function through the solution of the Laplace equation over the smallest box that contains all elements that are enriched for a crack (Laplace domain) with discontinuous Dirichlet and vanishing Neumann boundary conditions. The interaction of any two cracks is modeled by imposing zero Neumann boundary conditions along one crack in the Laplace domain of the other crack. The harmonic enrichment function reproduces the generalized Heaviside function in the interior of the crack and the junction function close to the branching/intersecting points. In the neighborhood of the crack-tip, the harmonic enrichment function resembles the discontinuous near-tip enrichment function that is used in the X-FEM. In the HX-FEM, the enrichment function is a piecewise polynomial over each subgrid element. Therefore, numerical integration of the weak form integrals over the enriched elements is done with tensor-product Gauss quadrature rules, and partitioning is not required. Quadrature study of the HX-FEM revealed that a 2×2 Gauss quadrature rule over each subgrid was adequate for higher-order elements with different levels of subgrid refinement. The rate of convergence of HX-FEM was studied for linear, quadratic and cubic elements—a rate of one-half was realized, in agreement with finite element theory for $\sqrt{r}$-singularities.

Several numerical examples were solved with HX-FEM and accurate stress intensity factors were obtained in all cases, which reveals that harmonic enrichment function can successfully be applied to complex crack configurations when there are multiple interacting/branched cracks.

Application of the HX-FEM to more complicated problems such as many edge cracks in a long strip-shaped plate [30] and especially tree-shaped cracks [31, 32], which have not yet been attempted using X-FEM, is promising. In the case of tree-shaped cracks, handling the branches and partitioning of the elements containing the junction points can become exponentially burdensome as the cracks grow and branch, whereas in the HX-FEM, the enrichment functions of all the branches can be handled similarly as long as the length of the branch is kept fixed.

ACKNOWLEDGEMENTS

S. E. Mousavi and N. Sukumar acknowledge the research support of the National Science Foundation through contract grants CMMI-0626481 and DMS-0811025 to the University of California at Davis. E. Grinspun is supported by the Sloan Foundation and the NSF (CAREER Award CCF-06-43268 and grants IIS-09-16129, IIS-05-28402, CNS-06-14770). The authors are also grateful to Ramón Rojas-Díaz for providing us with the boundary element solutions for the branched crack problem in Section 5.5.

REFERENCES

1. T. Belytschko and T. Black. Elastic crack growth in finite elements with minimal remeshing. *International Journal for Numerical Methods in Engineering*, 45(5):601–620, 1999.
2. N. Moës, J. Dolbow, and T. Belytschko. A finite element method for crack growth without remeshing. *International Journal for Numerical Methods in Engineering*, 46(1):131–150, 1999.
3. E. Béchet, H. Minnebo, N. Moës, and B. Burgardt. Improved implementation and robustness study of the X-FEM for stress analysis around cracks. *International Journal for Numerical Methods in Engineering*, 64(8):1033–1056, 2005.
4. P. Laborde, J. Pommier, Y. Renard, and M. Salaün. High-order extended finite element method for cracked domains. *International Journal for Numerical Methods in Engineering*, 64:354–381, 2005.

5. C. Daux, N. Moës, J. Dolbow, N. Sukumar, and T. Belytschko. Arbitrary branched and intersecting cracks with the extended finite element method. *International Journal for Numerical Methods in Engineering*, 48(12):1741–1760, 2000.
6. T. Belytschko, N. Moës, S. Usui, and C. Parimi. Arbitrary discontinuities in finite elements. *International Journal for Numerical Methods in Engineering*, 50:993–1013, 2001.
7. A. Simone, C. A. Duarte, and E. Van der Giessen. A generalized finite element method for polycrystals with discontinuous grain boundaries. *International Journal for Numerical Methods in Engineering*, 67:1122–1145, 2006.
8. C. A. Duarte, L. G. Reno, and A. Simone. A high-order generalized FEM for through-the-thickness branched cracks. *International Journal for Numerical Methods in Engineering*, 72:325–351, 2007.
9. G. Ventura. On the elimination of quadrature subcells for discontinuous functions in the extended finite-element method. *International Journal for Numerical Methods in Engineering*, 66:761–795, 2006.
10. D. J. Holdych, D. R. Noble, and R. B. Secor. Quadrature rules for triangular and tetrahedral elements with generalized functions. *International Journal for Numerical Methods in Engineering*, 73:1310–1327, 2008.
11. S. Natarajan, D. R. Mahapatra, and S. P. A. Bordas. Integrating strong and weak discontinuities without integration subcells and example applications in an XFEM/GFEM framework. *International Journal for Numerical Methods in Engineering*, 83:269–294, 2010.
12. S. E. Mousavi, H. Xiao, and N. Sukumar. Generalized Gaussian quadrature rules on arbitrary polygons. *International Journal for Numerical Methods in Engineering*, 82:99–113, 2010.
13. S. E. Mousavi and N. Sukumar. Generalized Gaussian quadrature rules for discontinuities and crack singularities in the extended finite element method. *Computer Methods in Applied Mechanics and Engineering*, 2010. DOI: 10.1016/j.cma.2010.06.031.
14. K. Park, J. P. Pereira, C. A. Duarte, and G. H. Paulino. Integration of singular enrichment functions in the generalized/extended finite element method for three-dimensional problems. *International Journal for Numerical Methods in Engineering*, 78(10):1220–1257, 2009.
15. S. E. Mousavi and N. Sukumar. Generalized Duffy transformation for integrating vertex singularities. *Computational Mechanics*, 45(2–3):127–140, 2010.
16. P. Kaufmann, S. Martin, M. Botsch, E. Grinspun, and M. Gross. Enrichment textures for detailed cutting of shells. *ACM Transactions on Graphics*, 28(3):50:1–50:10, 2009.
17. S. E. Mousavi, E. Grinspun, and N. Sukumar. Harmonic enrichment functions: A unified treatment of

multiple, intersecting and branched cracks in the extended finite element method. *International Journal for Numerical Methods in Engineering*, 2010. DOI: 10.1002/nme.3020.

18. F. L. Stazi, E. Budyn, J. Chessa, and T. Belytschko. An extended finite element method with higher-order elements for curved cracks. *Computational Mechanics*, 31(1–2):38–48, 2003.
19. K. W. Cheng and T. P. Fries. Higher-order XFEM for curved strong and weak discontinuities. *International Journal for Numerical Methods in Engineering*, 82:564–590, 2010.
20. M. H. Aliabadi, D. P. Rooke, and D. J. Cartwright. Mixed-mode Bueckner weight functions using boundary element analysis. *International Journal of Fracture*, 34:131–147, 1987.
21. A. Tabarraei and N. Sukumar. Extended finite element method on polygonal and quadtree meshes. *Computer Methods in Applied Mechanics and Engineering*, 197(5):425–438, 2008.
22. G. C. Sih. *Boundary Problems for Longitudinal Shear Cracks*. Pergamon, New York, 1964.
23. A. K. Yavuz, S. L. Phoenix, and S. C. TerMaath. Multiple crack analysis in finite plates. *AIAA Journal*, 44(11):2535–2541, 2006.
24. L. Brandinelli and R. Ballarini. Stress-intensity factor approximations for two-dimensional curvilinear cracks. *Composites Science and Technology*, 60:2557–2564, 2000.
25. Y. Murakami, editor. *Stress Intensity Factors Handbook*. Oxford: Pergamon Press, New York, 1987.
26. J. Englund. Fast, accurate, and stable algorithm for the stress field around a zig-zag-shaped crack. *Engineering Fracture Mechanics*, 70:355–364, 2003.
27. J. Niu and M. S. Wu. Strong interactions of morphologically complex cracks. *Engineering Fracture Mechanics*, 51(6):665–687, 1991.
28. S. C. TerMaath, S. L. Phoenix, and C.-Y. Hui. A technique for studying interacting cracks of complex geometry in 2D. *Engineering Fracture Mechanics*, 73:1086–1114, 2006.
29. F. García, A. Sáez, and J. Domínguez. Traction boundary elements for cracks in anisotropic solids. *Engineering Analysis with Boundary Elements*, 28:667–676, 2004.
30. J. Englund. A Nyström scheme with rational quadrature applied to edge crack problems. *Communications in Numerical Methods in Engineering*, 23:945–960, 2007.
31. J. Englund. Stable algorithm for the stress field around a multiply branched crack. *International Journal for Numerical Methods in Engineering*, 63:926–946, 2005.
32. G. W. Ma, X. M. An, H. H. Zhang, and L. X. Li. Modeling complex crack problems using the numerical manifold method. *International Journal of Fracture*, 156:21–35, 2009.